Excited state dynamics of Cl_2O in the near ultraviolet

Robert Aures, Karl-Heinz Gericke,[a] Christof Maul, and Gundula Trott-Kriegeskorte
Institut für Physikalische und Theoretische Chemie, Technische Universität Braunschweig, Hans-Sommer-Straße 10, D-38106 Braunschweig, Germany

Masahiro Kawasaki and Yukio Nakano
Department of Molecular Engineering, Kyoto University, Kyoto 606-8501, Japan

(Received 4 January 2002; accepted 7 May 2002)

The state-resolved and isotope-specific detection of nascent ClO generated from the photodissociation of Cl_2O parent molecules is performed by observing single-color $(2+1)$ resonance enhanced multiphoton ionization (REMPI) spectra following excitation in the wavelength range from 336 to 344 nm; additionally state-resolved detection of nascent ClO is performed by observing single-color two photon laser-induced fluorescence. The REMPI spectrum is assigned to the $ClO(C\,^2\Sigma^-, v'=0 \leftarrow X\,^2\Pi_\Omega, v=0)$ transition. The population of rotational states up to $J=130$ is evidence of large rotational excitation induced by a strong dependence of the excited potential energy surface (PES) on the Jacobi angle γ. Formation of the $^2\Pi_{3/2}$ spin-orbit state is preferred: $P(^2\Pi_{1/2}):P(^2\Pi_{3/2})=0.30\pm0.05$ suggesting significant radiationless transfer from the excited PES to closely lying neighboring states. The anisotropy parameter for the transition is determined to be $\beta=0.35$ independent of the ClO quantum state. The principal excited electronic state is assigned to a $^1B_2 \leftarrow {}^1A_1$ transition, in agreement with recent *ab initio* calculations. The measured β value is smaller than the limiting value of 1.0, suggesting dynamic reasons and simultaneous excitation to more than one PES. A fast and direct fragmentation process is deduced, where the upper limit for the lifetime of the excited dissociative state is calculated to be 300 fs. © *2002 American Institute of Physics.* [DOI: 10.1063/1.1489415]

I. INTRODUCTION

The oxides of chlorine play an important role in the stratospheric chemistry and particularly in the depletion of the ozone layer.[1–11] The molecular constants and ground state configuration of Cl_2O are summarized in Table I. Concerning the photodissociation of Cl_2O at short wavelengths ($\lambda \leqslant 308$ nm) a large number of experimental and theoretical data are available. Even though absorption cross sections (for $\lambda \geqslant 300$ nm) for many temporary reservoir species are small, photolysis is still the most important loss process for these molecules in the lower stratosphere. In order to complete our understanding of the photolysis of stratospheric temporary reservoir species, studies of their photodissociation beyond 308 nm are necessary.

Photofragmentation of Cl_2O is possible for excitation wavelengths below 868 nm. Five different decay channels are accessible in the ultraviolet (UV)/visible (VIS) spectral range:

$$Cl_2O \rightarrow Cl(^2P_J) + ClO(^2\Pi_\Omega),$$

$$D_0 = 11\,530\ \text{cm}^{-1}/\lambda_{thr} = 868\ \text{nm}, \tag{1a}$$

$$Cl_2O \rightarrow Cl_2(^1\Sigma_g^+) + O(^3P_J),$$

$$D_0 = 13\,710\ \text{cm}^{-1}/\lambda_{thr} = 729\ \text{nm}, \tag{1b}$$

$$Cl_2O \rightarrow Cl_2(^1\Sigma_g^+) + O(^1D_2),$$

$$D_0 = 29\,580\ \text{cm}^{-1}/\lambda_{thr} = 338\ \text{nm}, \tag{1c}$$

$$Cl_2O \rightarrow Cl_2(^3\Pi_0^+) + O(^3P_J),$$

$$D_0 = 31\,540\ \text{cm}^{-1}/\lambda_{thr} = 317\ \text{nm}, \tag{1d}$$

$$Cl_2O \rightarrow 2Cl(^2P_J) + O(^3P_J),$$

$$D_0 = 33\,710\ \text{cm}^{-1}/\lambda_{thr} = 297\ \text{nm}. \tag{1e}$$

The dissociation energies D_0 and threshold wavelengths λ_{th} have been calculated, based on 0 K enthalpy of formation data, for the spin-orbit states with the lowest energy [$J(\text{Cl}) = 3/2$, $J(\text{O}) = 2$, and $\Omega(\text{ClO}) = 3/2$].[12]

The Cl_2O absorption spectrum is depicted in Fig. 1. It is characterized by a continuous and structureless absorption with four different maxima of increasing intensities at 530 nm, 410 nm (A), 256 nm (C), and 171 nm (D). The maximum situated at 256 nm is accompanied by a shoulder at 285 nm (B). In view of the broad absorption spectrum it is important to characterize the excitation dynamics of Cl_2O with respect to the different absorption bands as well as to characterize the decay dynamics with respect to the competing photolytic channels (1a)–(1e). Channel (1a) is expected to be the only decay channel active at dissociation wavelengths above 338 nm, since channel (1b) is spin-forbidden, and its contribution is expected to be negligible for a fast fragmentation process.

Until recently studies of the Cl_2O photodissociation dynamics have only been performed for wavelengths below 310 nm (cf. Table II).[13–18] Only, Davis and Lee studied the photodissociation of Cl_2O at 423 nm probing maximum A in Fig. 1. Using photofragment translational spectroscopy

[a]Author to whom correspondence should be addressed. Electronic mail: k.gericke@tu-bs.de

TABLE I. Molecular equilibrium constants for ground state Cl_2O. r_e is the Cl–O equilibrium bond length, α_e defines the bond angle (cf. Fig. 7), ω_i $(i=1-3)$ defines the three vibrational mode energies, and $A-C$ are the rotational constants.

Symmetry group	C_{2v}
Ground state	$^1A_1$
r_e (pm)	169.587[a]
α_e (deg)	110.886[a]
ω_1 (cm^{-1})	641.9694[b]
ω_2 (cm^{-1})	296.0[c]
ω_3 (cm^{-1})	686.5396[b]
A (cm^{-1})	1.40[a]
B (cm^{-1})	0.12[a]
C (cm^{-1})	0.11[a]

[a]Reference 11.
[b]Reference 9.
[c]Reference 10.

TABLE II. Experimental and calculated anisotropy parameter β in the photodissociation of $Cl_2O+h\nu\rightarrow ClO+Cl$ for wavelength above 235 nm. Band designations (cf. Fig. 1) in parentheses indicate minor contributions of another band.

λ_{exc} (nm)	423	340	308	248	235
Band	A	B	$B(+C)$	C	C
β_{exp}	-1.0[a]	0.35 ± 0.15[b]	0.4 ± 0.3[c]	$0.7-1.5\pm0.3$[c,d]	1.2 ± 0.1[e]
					0.7 ± 0.2[f]
Symmetry[g]	$^1B_1$	$^1B_2$	$^1B_2$	$_1A_2/^1A_1$	$_1A_2/^1A_1$
β^*[h]	-1.0	$+1.0$	$+1.0$	$(-1.0)/0.0$	$(-1.0)/0.0$

[a]Reference 13.
[b]This work.
[c]References 14 and 15.
[d]Depending on fragment recoil velocity.
[e]Reference 16.
[f]References 17 and 18.
[g]Reference 21.
[h]β^* values are limiting values for prompt dissociation and identical ground and excited state geometries.

(PTS) for the Cl fragments they found the anisotropy parameter β to be -1.0.[13] Here, β characterizes the spatial fragment distribution $P(\theta)$ according to $P(\theta)\propto 1+\beta P_2(\cos\theta)$, where θ is the angle of the polarization vector of the dissociating laser with the product recoil velocity vector, and P_2 is the second Legendre polynomial.[19] Okumura and co-workers[14,15] performed PTS experiments for dissociation wavelengths of 308, 248, and 193 nm, probing maxima *B*, *C*, and *D* in Fig. 1. At 308 nm (cf. Table II), only Cl and ClO fragments from channel (1a) were observed, with a single broad kinetic energy distribution (KED) and a spatial fragment distribution that is described by a β parameter of 0.4 ± 0.3. At 248 nm, 96% of the total fragments were Cl $+$ClO from channel (1a), but the KED consisted of three distinct contributions. The fastest fragments were associated with a β value of 0.7 ± 0.2, the products at moderate recoil velocities were characterized by $\beta=1.5\pm0.3$, and the slowest fragments were described by $\beta=1.2\pm0.2$. The remaining 4% dissociated into three fragments, $2Cl(^2P_J)+O(^3P_J)$, along channel (1e). No contribution from channels (1b), (1c), or (1d) were observed. These observations led the authors to suggest the involvement of several excited states in the dissociation at 248 nm. At 193 nm, photolysis of Cl_2O leads predominantly to three atomic fragments.[14] The reported mean β parameter of 0.4 for the oxygen atom was derived from a two-point measurement only and should be used with some caution in view of the dominance of the three-body decay channel (1e).

Tanaka and co-workers performed a photofragment imaging experiment at a dissociation wavelength of 235 nm.[16] Production of ground state $Cl(^2P_{3/2})$ atoms is strongly preferred over the production of excited spin-orbit state $Cl^*(^2P_{1/2})$ atoms, described by a branching ratio $P(^2P_{1/2}):P(^2P_{3/2})$ of 0.08 ± 0.01. The spatial distribution is characterized by a single β parameter of 1.2 ± 0.1 for both fine-structure states, independently of the fragment velocity, indicating the same initially excited potential energy surface (PES) for the production of all atomic Cl fragments. While

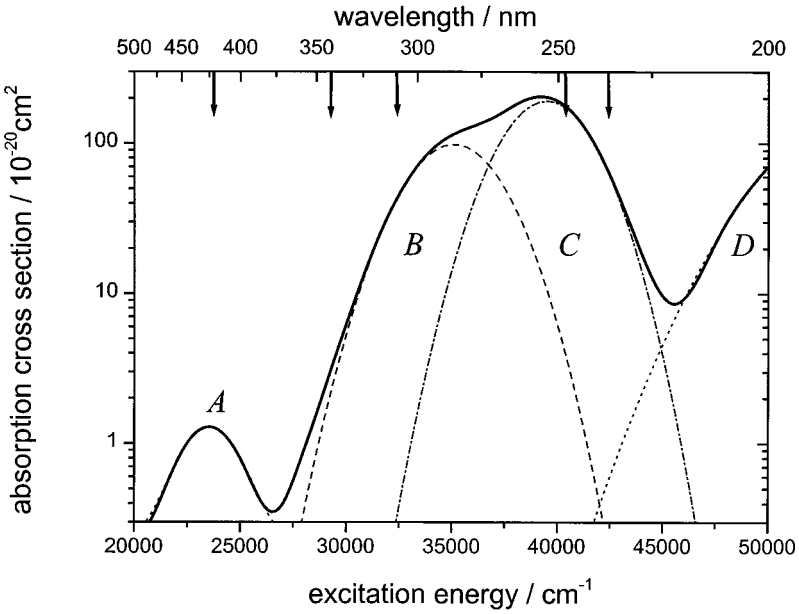

FIG. 1. Cl_2O absorption spectrum between 200 and 500 nm (solid line) (Ref. 26). Four Gaussian curves (*A*, *B*, *C*, *D*) fit this experimental spectrum (dashed lines). All results of the present study are related to the *B* band. Arrows indicate the different excitation wavelengths found in the literature (cf. Table II).

some discrepancies remain between the experiments performed at 248 nm and at 235 nm, especially with respect to the spatial fragment distribution, it seems plausible that the same upper PES is excited for both wavelengths, and that the differing dynamics is essentially caused by the amount of the initially deposited energy in the parent and by the accessed region of the PES. Above all, the contribution of the three-body decay channel (1e) is strongly increased.

Most recently, time-of-flight (TOF) experiments with resonantly enhanced multiphoton ionization (REMPI) detection of $Cl(^2P_{3/2})$ and $Cl^*(^2P_{1/2})$ were performed at dissociation wavelengths of 235 and 207 nm.[17,18] Qualitatively the previously obtained data for 235 nm were confirmed, whereas at 207 nm an almost isotropic decay was observed, characterized by $\beta=0.2\pm0.2$. Here, KEDs of predominantly slow atomic chlorine fragments are evidence of the three-body decay dominating the dissociation process, resembling the results obtained in the 193 nm dissociation. Contrary to the 235 nm dissociation, no spin-orbit state selectivity was observed. Clearly, another electronic state of different symmetry must be responsible for the Cl_2O dissociation in the D maximum in the wavelength region below 220 nm.

Few theoretical studies have been performed on the electronic states of Cl_2O.[5,20–22] Sander and co-workers[5] calculated vertical excitation energies and assigned the calculated states to the absorption spectrum maxima. The A maximum at 410 nm was assigned to a $^3B_1$ state, the B shoulder at 285 nm to the corresponding $^1B_1$ state, the C maximum at 256 nm to a $^1B_2$ state, and the D maximum to overlapping $^1A_1$ and $^1B_2$ states. This assignment was consistent with all the existing experimental observations compiled above, except for the observed β parameter at 308 nm and the unusually strong intercombination transition at 410 nm. In fact, other calculations[20–22] resulted in the assignment of the $^1B_1$ state to the A maximum and the neighboring $^1B_2$ state to the B shoulder. While the new calculations fixed the above mentioned discrepancies in the long wavelength regime, new discrepancies arose in the short wavelength part of the absorption spectrum which cannot be resolved at present.

Quantum state resolved data were only available for the atomic Cl fragment, whereas the quantum states of the ClO fragment containing the most detailed information about the dissociation process were unidentified. In a recent work we observed for the first time extremely high rotational excitation in the ClO fragments upon the photodissociation of Cl_2O around 340 nm via state-resolved REMPI.[23] The rotational population, derived by fitting a Gaussian distribution function to the obtained spectra, was strongly inverted peaking around $J=107.5$ having a full width at half maximum (FWHM) of 26.6. The extreme high rotational excitation agrees very well with the prediction of a purely impulsive model. Thus the gradient of the upper potential energy surface (PES) with respect to the separation coordinate must dominate the dependence on the Cl–O–Cl bond angle. This behavior should be typical for relatively large energy release in a bent heavy–light–heavy triatomic molecule.

A more detailed view on the dynamics evolving the excited PES and the nature of the excited state can be obtained by studying the spatial fragment anisotropy described by the β parameter, defined through the spatial fragment distribution $P(\theta)$. Based on semiclassical trajectory calculations, Persico and co-workers predicted a β parameter of 1.7 for dissociation on the $^1B_2$ surface.[22] Accessing a state of B_2 symmetry from an A_1 state yields a limiting β parameter of $+1.0$ for identical ground and excited state geometries (at a bond angle of 110.9°). An increase of β from the limiting value to higher values can only be due to the topology of the upper PES, whereas a decrease can be caused by more than one factor, i.e., excited PES topology, noninstantaneous dissociation or simultaneous excitation of different upper potential energy surfaces.

In this work we use the REMPI technique for ClO detection, which in combination with time-of-flight measurements allows us to study the spatial fragment distribution in detail and to extract the β parameter value to a high degree of accuracy. Additionally to the REMPI spectra, we measured state-resolved single-color two photon laser-induced fluorescence spectra (LIF) of ClO.

In contrast to conventional fluorescence spectroscopy the REMPI method offers various advantages: first, it is capable of distinguishing between signals from the two prominent ClO isotopes (^{35}ClO and ^{37}ClO).[24,25] Thus, isotopically pure spectra can be observed, greatly simplifying the complex ClO spectra and facilitating their interpretation. Second, inevitable impurities in the sample, especially ClO_2, that might contribute to the ClO signal yield, can be discriminated against, based on their difference in kinetic energy release to the fragments. The content of ClO_2 is especially crucial in this regard, since its absorption cross section around 340 nm is $\sigma=1.23\times10^{-17}$ cm^2, whereas the value of the absorption cross section for Cl_2O is only $\sigma=3.58\times10^{-20}$ cm^2.[26]

The present article describes the photodissociation of Cl_2O in the wavelength range from 336 to 344 nm leading to ClO+Cl products. For the photodissociation of Cl_2O, isotope selective spectra for ^{35}ClO and ^{37}ClO are measured and for the first time the anisotropy parameter β of the decay around 340 nm is determined. An upper limit for the lifetime of the excited dissociative state is given. The ClO fragment is completely characterized by its rotational and spin-orbit states using $(2+1)$ and $(2+2)$ REMPI.

II. EXPERIMENT

The Cl_2O dissociation dynamics are studied in a one-color experiment consisting of two elementary steps. First, Cl_2O is dissociated by absorbing one ultraviolet (UV) photon (between 336 and 344 nm). The resulting ClO fragment is then detected via a $(2+1)$ or a $(2+2)$ REMPI process, depending on the wavelength.[27,28] Ground state ClO ($X^2\Pi_\Omega$) is excited to the upper electronic C state ($C\,^2\Sigma^-\leftarrow X\,^2\Pi_\Omega$) by absorption of two UV photons and subsequently ionized by one or, respectively, two photons. At wavelengths above 342 nm the detection process changes from $(2+1)$ to $(2+2)$ REMPI. The REMPI technique allows a sensitive, isotope-selective and state-resolved observation of nascent ClO from the photodissociation process of Cl_2O when the dye laser is tuned from 336 to 344 nm. For reference, $(2+1)$ LIF spectra of ClO were measured by absorption of two UV photons

with subsequent monitoring of the vacuum–ultraviolet fluorescence from the excited electronic state to the ground state ($C\,^2\Sigma^- \rightarrow X\,^2\Pi_\Omega$) around 170 nm.

The linear TOF spectrometer is described in detail elsewhere.[29] Basically it consists of a stainless steel tube evacuated to a base pressure of 10^{-4} Pa equipped with quartz windows for photolysis and probe lasers traversing perpendicular to the single-field TOF spectrometer. For the preparation of gaseous dichlorine monoxide (Cl_2O) the method of Cady[30] was used. Remaining chlorine molecules in the sample were removed by vacuum distillation. The Cl_2O gas ($8\times10^3-13\times10^3$ Pa) was mixed with argon to a total pressure of 10^5 Pa. A pulsed nozzle (General Valve Series 9) was used to expand the gas mixture inside the spectrometer perpendicular to the spectrometer axis. Using repetition rates of 10 Hz and a stagnation pressure of 2×10^4 to 1×10^5 Pa we obtained a background pressure of about 10^{-2} Pa with the nozzle in operation.

Both the Cl_2O photolysis wavelength and the ClO detection wavelength in the range of 336 to 344 nm were delivered by the same tunable dye laser (FL 3002, Lambda Physik) pumped by a XeCl excimer laser (Radiant Dyes RD-EXC-200). p-Terphenyl (PTP) dissolved in dioxane was used as laser dye. The pulse duration was 15 ns and the dye laser output (RDC 360-neu) was 3–4 mJ/pulse at a bandwidth $\Delta\nu$ of 0.21 cm^{-1} (FWHM). The bandwidth was determined from the convolution procedure described below. The dye laser was focused by a $f=300$ mm quartz lens. Two microchannel plates (MCPs, Galileo Longlife) with an active diameter of 40 mm mounted in chevron position were used to detect the ions. For monitoring ClO spectra the output of the MCPs was fed into boxcar averager (Stanford Research Systems 250) and stored in a personal computer after analog/digital (A/D) conversion. Since the flight times of ^{35}ClO and ^{37}ClO differ due to their different masses, isotope-specific spectra were observed simultaneously by adjusting two boxcar gates at the respective arrival times while scanning the dye laser. The signals were normalized by measuring the probe laser intensity.

The experimental setup used for the state-resolved two-photon LIF bulk detection of ClO or BrO has been described in detail before.[31] A solar-blind photomultiplier (Thorn EMI 9403B), which is not sensitive to the excitation wavelength, was mounted perpendicular to the laser beam. The output of the photomultiplier was fed into a boxcar averager (Stanford Research Systems 250) and stored in a personal computer after A/D conversion.

For extracting β parameter values the transient TOF profile for a selected transition at a fixed laser wavelength was averaged over 1000 shots by a digital oscilloscope (LeCroy 9450 A, 350 MHz) and saved by a personal computer. The polarization of the laser was rotated by a prism assembly in order to investigate the spatial fragment distribution. Polarization geometries of $\eta=0°$ and 90° were realized where η is the angle of the polarization vector of the dissociation laser with the spectrometer axis. The β parameter was determined from a forward convolution procedure taking into account the spectrometer response function and the linewidth of the probe laser.

In order to account for the problem of unwanted ClO signals resulting from the small (1%) ClO_2 impurities in our samples the following experimental arrangement was employed. For a photolysis wavelength around 340 nm leading to ClO fragments, the available energy E_{av} of the dissociation for Cl_2O is about 1.8 times the value for ClO_2, where E_{av} has been calculated from the difference between the photon energy and the dissociation energy: E_{av} (ClO_2) $=10\,100\ cm^{-1}<E_{av}(Cl_2O)=17\,800\ cm^{-1}$. Additionally, the kinetic energy release into the fragments has to be weighted by the respective masses of the fragments. Therefore, TOF profiles for ClO generated from the dissociation of Cl_2O are significantly broader than profiles from the photolysis of ClO_2. The minimum ratio for the profile widths is calculated to be 1.7 in absence of internal fragment excitation. For internal ClO excitation this ratio will be even larger. Setting the gate of the boxcar integrator to the outer 30% of the wing of the TOF profile will thus ensure that only ClO from the dissociation of Cl_2O is measured. For the same reason contributions from signals originating from $Cl_2O_n \cdot Ar_m$ clusters can be excluded.

III. RESULTS

Purity of the sample is of major concern in the present experiment, especially in view of the small absorption cross section for Cl_2O at 340 nm ($\sigma=3.58\times10^{-20}$ cm^2).[26] Possible impurities comprise Cl_2, HOCl, and OClO. The sample composition was checked by monitoring an UV/VIS absorption spectrum which is depicted in Fig. 2. Indeed, all species discussed above were present in the sample which was found to consist of 33% Cl_2, 15% HOCl, 1% OClO, and 51% Cl_2O. The relatively large content of HOCl and Cl_2 does not interfere with the present experiment. The small content of OClO however, results in nonnegligible interference signals. Therefore, ClO spectra were monitored from integrating the high-speed part of the TOF profiles only where no ClO contribution from ClO_2 dissociation is present, as described in the previous section. Additionally, ClO_2 dissociation is known to predominantly generate ClO fragments in low rotational states, whereas Cl_2O dissociation mainly produces highly rotationally excited fragments.[23,31] Arguments based on the rotational excitation of ClO are, therefore, not influenced by ClO_2 impurities in the sample.

A. Quantum state population

An overview over the observed ClO REMPI and LIF spectra resulting from the one-color experiment in the dissociation of Cl_2O is represented in Fig. 3. The upper part shows the LIF spectrum of ClO whereas the middle and lower part of the figure depicts the REMPI spectra for the ^{37}ClO and ^{35}ClO isotope. Note the scaling of the signal intensities in the isotope selective REMPI spectra, which reflects the natural abundance ratio of 1:3. The scan range from 336 to 344 nm covers the rotational branches of ClO ($C\,^2\Sigma^-, v'=0 \leftarrow X\,^2\Pi_{3/2}, v=0$) and ClO ($C\,^2\Sigma^-, v'=0 \leftarrow X\,^2\Pi_{1/2}, v=0$). The onset of the $^2\Pi_{3/2}$ system at 341.6 nm is indicated by the bandheads of the *P* and *O* branches. The other spin-orbit system, $^2\Pi_{1/2}$, starts at about 343.6 nm. At room temperature both electronic systems are well separated

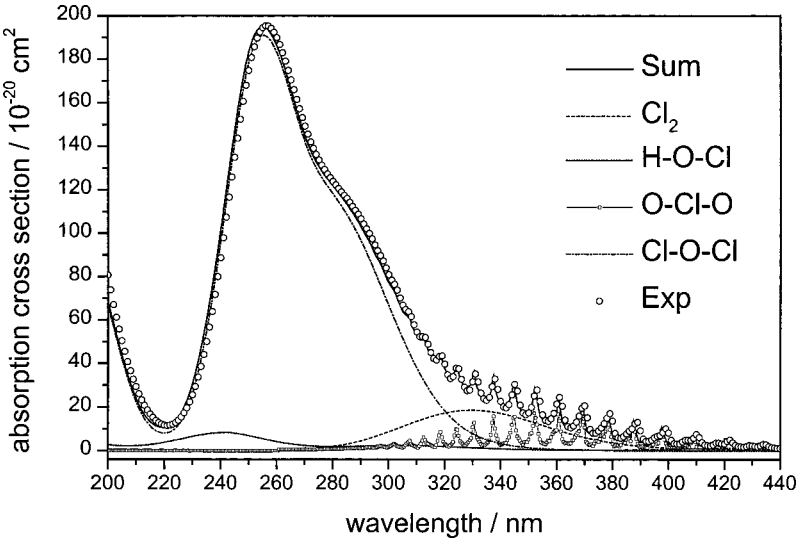

FIG. 2. UV/VIS absorption spectrum of the Cl_2O sample used for the experiments. Measured absorption spectra (open circles) reflect the chemical composition of the sample given by the sum (solid line) of the impurities and the Cl_2O content, namely 33% Cl_2 (short dash), 15% HOCl (dot), 1% OClO (open square symbol), and 51% Cl_2O (short dash dot). Data for the absorption spectra of the pure substances are taken from Ref. 26.

($A_0 = -321.79\ \mathrm{cm}^{-1}$).[32] In the Cl_2O dissociation, due to the high rotational excitation, transitions from high rotational states of the $^2\Pi_{1/2}$ system overlap with transitions from the $^2\Pi_{3/2}$ system.[23] High rotational excitation is also present in excited vibrational states of ClO obscuring the bandheads of the $^2\Pi_{1/2}$ system at 343.6 nm in the overview of Fig. 3. The origin of the heavy isotope is redshifted by 0.96 cm^{-1} from the origin of the ^{35}ClO isotope ($T_e = 58\,374.73\ \mathrm{cm}^{-1}$). The molecular constants for ^{37}ClO were calculated using the constant $\rho = [\mu(^{35}\mathrm{ClO})/\mu(^{37}\mathrm{ClO})]^{1/2}$, i.e., the square root of the ratio of the reduced masses μ.[33]

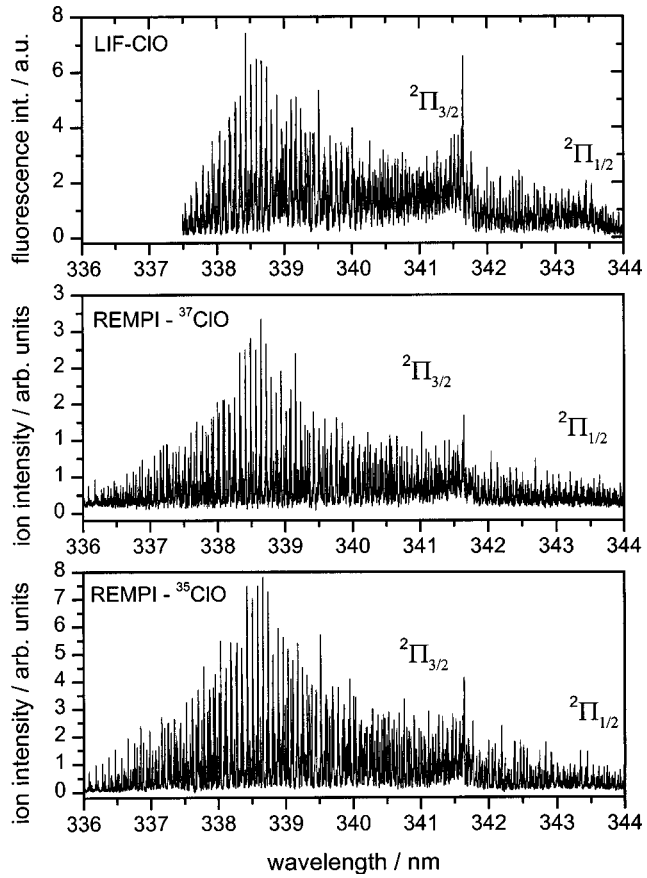

FIG. 3. Nascent two-photon REMPI spectra of ^{37}ClO and ^{35}ClO and LIF spectra of ClO in the one-color photodissociation study of Cl_2O between 336 and 344 nm. The spectra represent rotational branches of the (0-0) vibrational transitions of ClO($C\,^2\Sigma^- \leftarrow X\,^2\Pi_{3/2}$) and ClO($C\,^2\Sigma^- \leftarrow X\,^2\Pi_{1/2}$). The bandheads for the two spin manifolds are marked.

The removal of interferences from ClO_2 impurities can best be seen in the amplitude ratio of the intense *P* bandhead at 341.69 nm. The LIF spectrum contains significantly more population of low rotational states contributing to the bandhead from the REMPI spectrum. The difference is ascribed to ClO fragments resulting from the photodissociation of ClO_2 impurities, which are not monitored in the REMPI experiment due to the energy sensitive gating procedure described in Sec. II.

In our recent work, related to ^{35}ClO, we have shown that the population of the high rotational states is strongly inverted described by a Gaussian distribution peaking at $J = 107.5$ with a FWHM of $\Delta J = 26.6$.[23] The new REMPI spectra for ^{37}ClO and the LIF spectra, presented in this work, confirm our previous findings.

Whereas around 340 nm transitions belonging to rotational levels of ClO ($v = 0$) are excited, for excitation around 346 nm, higher vibrational levels of ClO are responsible. However, the intensity of the dye laser around this wavelength is very low and the REMPI detection scheme changes from $(2+1)$ to $(2+2)$ detection. Both effects are responsible for the result that REMPI measurements at wavelengths beyond 344 nm were not possible. However, our recent LIF data confirm a population of vibrational states up to ($v = 3$) with significant rotational excitation of the ClO fragments. Due to the complex structure of the LIF spectra no quantitative vibrational populations could be extracted.

The population ratio of the two spin-orbit manifolds $P(^2\Pi_{1/2}):P(^2\Pi_{3/2})$ is obtained from the REMPI spectra for ^{35}ClO and ^{37}ClO from evaluating the bandhead intensities of the $^2\Sigma^- \leftarrow ^2\Pi_{3/2}$ and $^2\Sigma^- \leftarrow ^2\Pi_{1/2}$ transitions. The ratio is given by $P(^2\Pi_{1/2}):P(^2\Pi_{3/2}) = 0.30 \pm 0.05$ for both isotopes. The experimental value of 0.30 is evidence for a preferred formation of the $^2\Pi_{3/2}$ component.

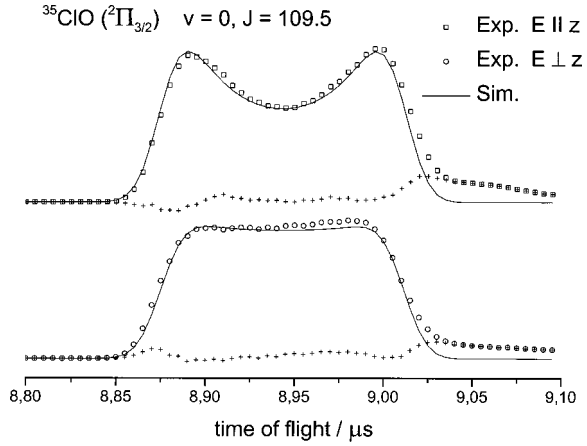

FIG. 4. Experimental and simulated TOF profiles for ^{35}ClO obtained at a dissociation wavelength of 338.27 nm. Squares represent experimental profiles observed with a parallel alignment (**E**∥**z**) between laser polarization **E** and the spectrometer axis **z**. Circles represent measurements for perpendicular alignment (**E**⊥ **z**), respectively. The simulation is given by the solid line. Crosses represent the difference between experiment and simulation. The β parameter is determined to be 0.35 ± 0.15.

B. Spatial fragment anisotropy

A typical TOF profile for a selected rotational transition of ^{35}ClO($^2\Pi_{3/2}$) is shown in Fig. 4, which depends on the orientation of the laser polarization **E** with respect to the spectrometer axis **z**. Different shapes for parallel ($\eta = 0°$) and perpendicular ($\eta = 90°$) polarization geometries are observed. In the perpendicular case the projection of the velocity distribution is rectangular in shape, whereas in the parallel case, the wings of the profiles are enhanced. Thus, the velocity of the ClO fragments is mainly aligned parallel to the polarization vector **E** and the transition dipole moment $\boldsymbol{\mu}$. The TOF profiles $F(t)$ are proportional to the distribution $F(v_z)$ of the velocity component v_z along the spectrometer axis reflecting the projection of the three-dimensional velocity distribution onto the spectrometer axis **z**. For a single-valued velocity distribution, as is realized for the ClO fragment from the Cl_2O photodissociation, the projection is described by

$$F(v_z) = \frac{1}{2v_0}\left[1 + \beta \cdot P_2\left(\frac{v_z}{v_0}\right) \cdot P_2(\cos\eta)\right], \qquad (2)$$

where v_0 represents the absolute value of the velocity.[34] η is the angle between the spectrometer axis **z** and the polarization vector **E**. $P_2(x)$ is the second Legendre polynomial of x. Figure 4 depicts the best fits to the experimentally observed profiles for $\eta = 0°$ and $\eta = 90°$, taking into account the experimental response function of 25 ns and the laser linewidth of 0.21 cm^{-1}. The latter was incorporated into the fitting scheme to account for incomplete detection of ClO fragments due to large Doppler broadening of the ClO transition: the maximum kinetic energy release into the ClO fragment of 7330 cm^{-1} corresponds to a full width Doppler broadening of 0.36 cm^{-1}, which is clearly broader than the laser linewidth. This linewidth effect is also responsible for the almost rectangular shape of the lower trace (perpendicular polarization geometry) in Fig. 4 where a center peak would be expected for complete fragment excitation. Both profiles in Fig. 4 have simultaneously been fitted with the same β parameter. The cross symbols represent the difference between experiment and simulation. The somewhat larger residuals for large flight times (>9 μs) are caused by the ^{37}ClO isotope. Thus, the agreement with the experimental profiles is excellent and a β parameter of 0.35 ± 0.15 was determined. Various profiles at different dissociation wavelengths were fitted independently but the anisotropy parameter β was found to be the same $\beta = 0.35 \pm 0.15$.

The recorded line profiles shown in Fig. 4 were excited in the $^oO_{11}$ rotational band ($J = 109.5 \rightarrow 107.5$) at 338.27 nm. The observed flight times confirm the high rotational excitation of the ClO fragment observed via REMPI and LIF measurements: The TOF profile width of 140 ns corresponds to a ClO fragment speed $v_0 = 1330$ ms, i.e., to a kinetic energy of $E_{kin}(ClO) = 3770\ cm^{-1}$. Conservation of linear momentum yields a kinetic energy of $E_{kin}(Cl) = 5490\ cm^{-1}$ for the chlorine atom, in the Cl_2O center of mass frame. The available energy $E_{av}(ClO)$ of the ClO fragment is calculated as the difference from the photon energy $h\upsilon = 29\,560\ cm^{-1}$ and the dissociation energy $D_0 = 11\,530\ cm^{-1}$ to be $E_{av}(ClO) = 18\,030\ cm^{-1}$. The internal energy $E_{int}(ClO) = 8770\ cm^{-1}$ is deduced from the subtraction of the kinetic energy of Cl and ClO from the available energy. For ClO($^2\Pi_{3/2}, v = 0$) E_{int} is only due to ClO rotation, and a rotational quantum number $J = 119.5$ is calculated from the constants $B_u = 0.620\,51\ cm^{-1}$, $D_u = 1.328 \times 10^{-6}\ cm^{-1}$, and $H_u = -5.00 \times 10^{-13}\ cm^{-1}$ cited in our previous work.[23] A very good agreement is found for the J values derived from two independent measurements of the same fragment, namely from the spectroscopic determination in the REMPI spectrum and from kinematic reasoning based on the TOF experiments.

IV. DISCUSSION

In the UV/VIS spectral range ClOCl shows a broad and structureless spectrum indicating a fast and presumably direct decay. The present one-color REMPI photodissociation study has been performed beyond the prominent absorption band, which peaks at 256 nm. Figure 1 depicts a measured absorption spectrum[26] (solid line) and multiple Gaussian fits in order to represent possible electronic transitions, where the absorption bands are numbered by *A*, *B*, *C*, and *D*. The complexity of the spectrum is caused by the promotion of one of the nonbonding electrons of the Cl atoms to an O–Cl antibonding molecular orbital, accounting for various excited states of different symmetry in the molecule. With respect to the spatial distribution of the products (cf. Table II) recent experimental results[13–18] are contradictory in the assignments of the electronic excited states.[5,20–22] Whereas the *A* band in the Cl_2O absorption spectra around 410 nm was assigned by Nicolaisen *et al.*[5] to a triplet excited state ($^3B_1$), the groups of Del Bene *et al.*[20] and Toniolo *et al.*[21] assign this transition to a singlet excited state of $^1B_1$ symmetry. For wavelengths higher than 300 nm the theoretical predictions are confirmed by the experiments, yet for higher excitation energies the measured anisotropy parameters contradict theory (cf. Table II).

The complex spectrum of the two-photon (0–0) transition in Fig. 3 consists of 20 main and satellite branches. Regarding the smallness of the spin-splitting constant $\gamma = -0.0129\ \mathrm{cm}^{-1}$ of the upper $^2\Sigma$ state, the one-photon laser linewidth of 0.21 cm^{-1} and the intensity ratios for main and satellite lines, it is not expected that the satellite lines are resolvable for low J quanta ($J<30$). Thus, neglecting the overlap of the $^2\Pi_\Omega$ spin manifolds, the spectrum below 341.6 nm ($^2\Pi_{3/2}$ bandhead) is contributed to by six resolvable branches, namely the $^oO_{11}$, $^pP_{11}(^pO_{21})$, $^qQ_{11}(^qP_{21})$, $^rR_{11}(^rQ_{21})$, $^sS_{11}(^sR_{21})$, and $^tS_{21}$ branches where satellite branches overlapping with the respective main branches are given in parentheses (notation $^{\Delta N}\Delta J_{F'F''}$). In our recent work we have simulated the spectrum, obtaining a nonthermal rotational distribution, where ^{35}ClO is essentially found in rotational states above $J=90$. Rotational excitation up to $J=130.5$ was found, for which about 71% of the total rotational population of ClO is situated in between the FWHM limits of a Gaussian distribution ($94.5<J<120.5$).

A. Excited potential energy surface

For the measured REMPI spectra Cl_2O was excited in the B band. The assignment of this band has been subject to dispute in the literature.[5,20–22] However, the Cl_2O ground state configuration is well established due to both *ab initio* calculations[5,20–22] and photoelectron spectroscopy:[35,36]

$$X^1A_1[A']:\ \ldots(2a_2)^2(9a_1)^2(7b_2)^2(3b_1)^2(10a_1)^0(8b_2)^0,$$

where C_{2v} symmetry notation has been used. The symmetry representation in C_s is given in brackets. Both unoccupied ($10a_1$) and ($8b_2$) molecular orbitals (MOs) are Cl–O antibonding. All occupied MOs given above are Cl–O nonbonding linear combinations of Cl ($3p$) atomic orbitals.

The following eight possible excited states arise from single electronic transitions:

$$A_1[A']:\ \ldots(2a_2)^2(9a_1)^2(7b_2)^1(3b_1)^2(10a_1)^0(8b_2)^1,$$

$$A_1[A']:\ \ldots(2a_2)^2(9a_1)^1(7b_2)^2(3b_1)^2(10a_1)^1(8b_2)^0,$$

$$A_2[A'']:\ \ldots(2a_2)^2(9a_1)^2(7b_2)^2(3b_1)^1(10a_1)^0(8b_2)^1,$$

$$A_2[A'']:\ \ldots(2a_2)^1(9a_1)^2(7b_2)^2(3b_1)^2(10a_1)^1(8b_2)^0,$$

$$B_1[A'']:\ \ldots(2a_2)^2(9a_1)^2(7b_2)^2(3b_1)^1(10a_1)^1(8b_2)^0,$$

$$B_1[A'']:\ \ldots(2a_2)^1(9a_1)^2(7b_2)^2(3b_1)^2(10a_1)^0(8b_2)^1,$$

$$B_2[A']:\ \ldots(2a_2)^2(9a_1)^2(7b_2)^1(3b_1)^2(10a_1)^1(8b_2)^0,$$

$$B_2[A']:\ \ldots(2a_2)^1(9a_1)^1(7b_2)^2(3b_1)^2(10a_1)^0(8b_2)^1.$$

In the present experiment the spin-orbit distribution of ClO, $P(^2\Pi_{1/2})$, and $P(^2\Pi_{3/2})$, has also been determined: $P(^2\Pi_{1/2})/P(^2\Pi_{3/2})=0.30\pm0.05$. As can be seen in Fig. 5 all states which can be directly excited in the visible or near UV ($^1B_1, ^1B_2, ^1A_1$) correlate only with $Cl(^2P_J)+ClO(^2\Pi_{3/2})$. Only the $^1A_2$ state correlates with the formation of $Cl(^2P_J)+ClO(^2\Pi_{1/2})$. Therefore, an exclusive formation of $ClO(^2\Pi_{3/2})$ would be expected for a pure adiabatic decay. The excitation probability of the dipole-forbidden transition into the $^1A_2$ state is very small because it becomes allowed only by antisymmetric Cl–O–Cl stretch motion. Thus, observation of a significant amount of $ClO(^2\Pi_{1/2})$ indicates spin-orbit interaction during the decay or a transition to the $^1A_2$ surface from the initially excited PES, the latter being the likely cause for spin-orbit excitation in view of the proximity of the excited states (cf. Fig. 5).

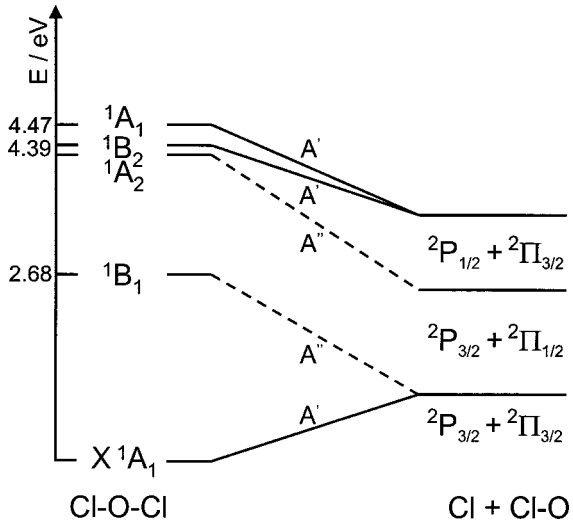

FIG. 5. Correlation diagram for the fragmentation of Cl_2O into Cl+ClO. Adiabatic correlations were taken from Tanaka *et al.*, (Ref. 16); the given energies were calculated by Toniolo *et al.* (Ref. 21). The $^1B_2$ and $^1A_2$ states are degenerate within accuracy of the calculations. Only the $^1A_2$ state, which cannot be reached via a dipole transition in C_{2v} geometry (cf. Fig. 6) correlates with ClO products in the $^2\Pi_{1/2}$ state.

B. Upper potential energy surface dynamics

The transition dipole moment μ for the $A_1 \leftarrow A_1$ transitions must be totally symmetric and, therefore, lies in the molecular plane bisecting the Cl–O–Cl bond angle α (cf. Figs. 6 and 7). For an instantaneous decay, based on ground state geometry, the angle φ of the ClO recoil vector **v** with the transition dipole moment μ is 55.4°. From this value a limiting β^* anisotropy parameter of 0.0 is expected according to

$$\beta^* = 2 \cdot P_2(\cos\varphi), \tag{3}$$

where P_2 is the second Legendre polynomial.[37] The $A_2 \leftarrow A_1$ transitions are symmetry-forbidden, but become allowed upon excitation of the antisymmetric stretch mode ν_3. The molecule symmetry is accordingly reduced from C_{2v} to C_s, with A'' symmetry for the excited state and A' symmetry for the ground state, respectively. The transition dipole moment $\mu(\mathbf{A}'')$ lies perpendicular to the molecular plane (i.e., $\varphi=90°$, cf. Fig. 6) and the limiting value β^* becomes -1.0. For the $B_1 \leftarrow A_1$ transitions the dipole moment is of b_1 symmetry. The situation is analogous to the A_2 case discussed above, giving the same limiting value of $\beta^*=-1.0$. Finally, the $B_2 \leftarrow A_1$ transitions are associated with a dipole moment of b_2 symmetry. Here, $\mu(\mathbf{A}')$ lies parallel to the line connecting the two Cl atoms in the molecular plane, forming an angle of $\varphi=34.6°$ with the recoil vector **v**, for an instantaneous decay in ground state geometry. Hence, the limiting value β^* for the anisotropy parameter is calculated to be $+1.0$. Out of the eight possible transitions above, only the

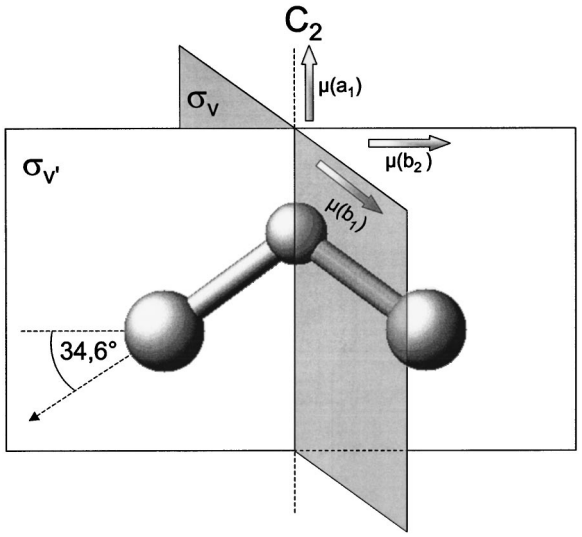

FIG. 6. C_{2v} geometry of ClOCl and alignment of transition dipole moments μ, which allow a characterization of the spatial distribution of ClO and Cl products. The Cl–O–Cl bond angle is 110.9°. For an instantaneous decay alignment of the transition dipole moment μ along the C_2 symmetry axis (a_1) forms an angle φ of 55.4° with the Cl fragment recoil velocity; alignment of μ in the molecular plane (b_2) corresponds to $\varphi=34.6°$, and alignment of μ perpendicular to the molecular plane (b_1) corresponds to $\varphi=90°$. The limiting values for the corresponding β^* parameters are 0.0, +1.0, and −1.0, respectively.

two $B_2 \leftarrow A_1$ transitions will lead to a positive β parameter, while the $A_2 \leftarrow A_1$ and $B_1 \leftarrow {}^1A_1$ transitions cause a negative and the $A_1 \leftarrow A_1$ transition a vanishing β value.

The experimentally observed dependence of the TOF profiles at 338.27 nm on the polarization of the photolysis laser is evidence for the anisotropic behavior, which can be employed to determine the orientation of the transition dipole moment μ and thus the symmetry of the excited state. The observed positive β parameter value of 0.35 ± 0.15 is in qualitative agreement with the calculations of Collaveri *et al.*[22] Thus, the state excited in our experiments around 340 nm is assigned to be of B_2 symmetry. Since the wavelength ($\lambda=338.27$ nm) used in our experiments, is on the red side of the proposed *B* band (cf. Fig. 1) the respective electronic configuration is $B_2[A']:\ldots(3b_1)^2(10a_1)^0(8b_2)^1$. Table II summarizes the electronic state assignments drawn from experiments and theory. Clearly, the transitions responsible for the *A* and *B* bands can be assigned to ${}^1B_1$ and ${}^1B_2$ symmetry.

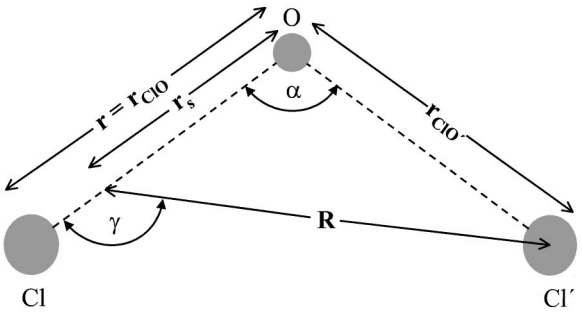

FIG. 7. Jacobi coordinates *r*, *R*, and γ and their relation to the natural coordinates r_{ClO}, $r_{\mathrm{ClO}'}$, and α for the Cl_2O molecule. r_s denotes the distance between the central O atom and the center of mass of the ClO diatom.

The experimental findings for the nature of the excited states, responsible for short wavelength transitions (*C* band), are in contradiction to theory. Collaveri *et al.*, however, recently explained this mismatch in terms of small errors in the computation of the excitation of the ${}^1B_2$ state. A displacement of its energy of about 0.2 eV would force the combined anisotropy β of the three excited states (${}^1A_2$, ${}^1B_2$, and ${}^1A_1$, cf. Fig. 5) to remain positive up to 235 nm, thus qualitatively confirming the experiments.

The observed reduction of the experimentally derived anisotropy parameter β from the calculated limiting β^* value can either be explained by nuclear motion of the parent during fragmentation or by simultaneous excitation of states of different symmetry. In detail three processes have to be considered: first, the reduction of the observed β parameter may be induced by parent rotation during the lifetime τ of the dissociative state.[38] Second, β may be influenced by the parent geometry change due to the topology of the excited PES characterized by $(\partial V/\partial\alpha)$. Finally, the simultaneous excitation of states with different symmetry will also influence the value of β.

Busch and Wilson give the following relation for the reduction of the anisotropy parameter from the limiting value β^* to the experimentally observed value β:

$$\beta = P_2[\cos(\omega\cdot\tau)]\cdot\beta^*, \tag{4}$$

where ω is the rotational angular frequency of the parent molecule and τ is the lifetime of its excited dissociative state.[38] For our case the value for ω was estimated to be 3.6×10^{11} Hz, based on a molecular beam sample temperature of $T_{\mathrm{rot}}=15$ K and the relevant rotational constant *C* being 0.11 cm^{-1} (cf. Table I).[11] The product term $\omega\cdot\tau$ describes the angle of rotation of the parent molecule in the time period between photon absorption and molecular decay. In principle, the effect of the tangential velocity associated with parent rotation also has to be considered, but can be neglected here due to its smallness. Insertion of the observed β value of 0.35 in relation (4) leads to a value of $\tau=300$ fs. This value is an upper limit for the lifetime of the excited state, but in agreement with previous experimental and theoretical work, the dissociation of Cl_2O is expected to be direct and fast with a significantly shorter lifetime than 300 fs. It should be noted however, that for a bulk experiment on room temperature Cl_2O the observed β parameter is reduced to 30% of the limiting value β^* after a period as short as 100 fs, due to the increased angular rotation frequency ω.

Second, the reduction of the β parameter can also be induced by the gradient $(\partial V/\partial\alpha)$ on the upper PES, with respect to the Cl–O–Cl bond angle α (cf. Fig. 7), favoring small bond angles. If this effect were solely responsible for the experimentally observed β parameter, then the Cl–O–Cl bond angle of the decay geometry would have to be 84.2°. A change of sign of $(\partial V/\partial\alpha)$ could even increase the β value, which clearly contradicts the experimental observation. Therefore, we conclude that the sign of the gradient $(\partial V/\partial\alpha)$ is positive preferring smaller bond angles on the upper PES. The magnitude of $(\partial V/\partial\alpha)$ is expected to be small, however, due to the minor contribution of the dynamically induced

torque on the rotational excitation of the ClO fragment, as was discussed in some detail above. This expectation agrees well with the calculations by Persico and co-workers who also found only a weak dependence of the upper PES on the natural bond angle α.[22] Thus, it is doubtful whether the geometry change is mainly responsible for the experimentally observed reduction of the β parameter. In this context the role of states of different symmetry needs to be discussed in more detail.

The last effect that can reduce the observed β parameter is the simultaneous excitation of different excited states belonging to different irreducible symmetry representations. Partial admixture of $A_1 \leftarrow A_1$ ($\beta^*=0$) and $A_2 \leftarrow A_1$ ($\beta^*=-1$) transitions to the main $B_2 \leftarrow A_1$ ($\beta^*=+1$) transition would reduce the observed value for β (cf. Table II). Both transitions exhibit a slightly higher vertical excitation energy (cf. Fig. 5) and should, therefore, become most important for dissociation at shorter wavelengths within the B feature of the observed spectrum. However, here, the magnitude of the oscillator strengths f for the different transitions are of importance. Whereas all theoretical and experimental work agrees that the $B_2 \leftarrow A_1$ transition is the most important one, calculated ratios for f vary from 5 to 200 for $B_2 \leftarrow A_1$ and $A_1 \leftarrow A_1$ transitions.[5,20–22] In general, it is difficult to calculate small oscillator strengths, so taking into account that the excitation energies of these three transitions are slightly different, simultaneous excitation of different states is a possible explanation of a significant reduction of β, at least for selected wavelength ranges. Following the argument above, for higher excitation energies one would expect the β parameter to be reduced more efficiently due to simultaneous excitation of different states than for long excitation wavelengths. Clearly, the experimental evidence summarized in Table II does not support this reasoning. Thus, a combination of the above discussed effects must be responsible for the observed anisotropy behavior. For short wavelength dissociation in the B region of the absorption spectrum a different weighting of the single effects is likely to occur. Possibly, oscillator strengths and vertical excitation energies might have to be adjusted slightly.

The reason for the observed high rotational excitation is the repulsion of the recoiling Cl fragment, as discussed in our previous work.[23] Other effects from overall rotation of the parent molecule in the electronic ground state, and bending vibration within the parent molecule can be excluded, since our experiments were measured under molecular beam conditions. Since a previous determination of the rotational temperature of the jet-cooled sample yielded a value of $\approx$10 K for phosgene expansion seeded in argon, we assume a similar rotational temperature for Cl_2O. Dynamic induction of rotational energy onto the diatomic fragment generated from the photodissociation of a triatomic parent molecule must be viewed in Jacobi coordinates r, R, and γ (cf. Fig. 7). Here, r is the internuclear distance in the diatomic, characterizing vibrational excitation, R is the distance between the atomic fragment and the center of mass of the diatomic characterizing the separation dynamics, hence the translational energy of the system, and γ denotes the angle of r with R, thus characterizing the rotation of the diatomic. For ClO the Jacobi coordinates r, R, and γ relate to the natural coordinates (r_{ClO}, $r_{Cl'O}$) and α as depicted in Fig. 7:

$$r = r_{ClO},$$

$$R = (r_s^2 + r_{Cl'O}^2 - 2r_s \cdot r_{Cl'O} \cdot \cos\alpha)^{0.5},$$

$$\gamma = \arcsin(r_{Cl'O} \cdot R^{-1} \cdot \sin\alpha),$$

where r_{ClO} and $r_{Cl'O}$ are the distances between the central O atom and the terminating Cl atoms, r_s is the distance between the central O atom and the center of mass of the ClO diatom and α is the bond angle. Cl′ denotes the departing atom whereas Cl remains bound to O in the ClO fragment. The amount of rotational excitation can be evaluated by integrating the gradient $F_\gamma = -(\partial V/\partial\gamma)$ of the upper PES along the dissociation coordinates; F_γ can be separated into two parts:[39]

$$F_\gamma = -\left(\frac{\partial V}{\partial r_{Cl'O}}\right)\cdot\left(\frac{\partial r_{Cl'O}}{\partial\gamma}\right) - \left(\frac{\partial V}{\partial\alpha}\right)\cdot\left(\frac{\partial\alpha}{\partial\gamma}\right) = F_\gamma^{(1)} + F_\gamma^{(2)}, \tag{5}$$

where the first part describes the rotational excitation induced by ClO repulsion (impulsive model) and the second part accounts for dynamical effects on the upper PES. Often the dynamic part $F_\gamma^{(2)}$, i.e., the bond angle dependence of the upper PES, dominates the rotational angular momentum transfer onto the diatomic products. However, especially for a triatomic parent molecule with a light central and two heavy terminating atoms like Cl_2O, the impulsive part $F_\gamma^{(1)}$ becomes more important due to a large value of $(\partial r_{Cl'O}/\partial\gamma)$. Thus, estimating the impulsive part

$$F_\gamma^{(1)} = -\left(\frac{\partial V}{\partial r_{Cl'O}}\right)\cdot\left(\frac{\partial r_{Cl'O}}{\partial\gamma}\right)$$

and its comparison to the experimentally observed rotational excitation will help to shed some light on the dynamics of the process. Calculated *ab initio* PES (Ref. 22) suggest a gradient of the upper PES with the natural dissociation coordinate of 0.04 eV/pm, which lets us calculate the torque $F_\gamma^{(1)}$ as a function of the Jacobi angle γ. Integration of $F_\gamma^{(1)}$ over the total change of γ during the decay yields an estimate for the rotational energy, while the torque asymptotically approaches 0 for $R \rightarrow \infty$. We derive a rotational energy of 1.91 eV, which corresponds to an angular momentum J of 157.5. Taking into respect that the recoil velocity of the Cl fragment is about 2.0 pm/fs, the dissociation process has to be completed within about 50 fs.

Since the calculated value for the impulsively induced rotational excitation is in the order of the experimentally observed excitation, the dynamic part $F_\gamma^{(2)}$ merely serves as a correction term to $F_\gamma^{(1)}$ accelerating or decreasing the rotational motion of the diatomic depending on the sign of $(\partial V/\partial\alpha)$. The value for the expression $(\partial\alpha/\partial\gamma)$ only depends on the molecular geometry and was calculated to be 1.24. Unfortunately, no quantitative data for $(\partial V/\partial\alpha)$ are available up to now, but from the arguments mentioned above we conclude that for Cl_2O the dynamic contribution is small. For comparison the pure impulsive model, which completely neglects the topology of the upper PES, yields, for the available

energy of 2.2 eV, a value of 0.96 eV for E_{rot}, respectively, $J=112.5$. Thus, our experimental findings suggest a positive sign for the gradient $(\partial V/\partial\alpha)$, reducing the torque F_γ. Persico and co-workers[22] calculated a β parameter of 1.7 for the decay on the B_2 surface, for excitation around 340 nm, based on quasi-classical trajectory calculations, thus suggesting a negative sign for the gradient $(\partial V/\partial\alpha)$. This quantitative contradiction remains to be clarified in future investigations.

V. CONCLUSION

For the first time, isotope- and state-specific spectra of ClO generated in the near UV photodissociation of Cl_2O have been measured by one-color $(2+1)$ and $(2+2)$ REMPI under background-free conditions. Additionally state-specific LIF spectra were recorded. The qualitative behavior of the upper potential surface of Cl_2O was determined by state-resolved detection of the $ClO(X\,^2\Pi_{\Omega,v,J})$ product at photolysis wavelengths between 336 to 344 nm. High rotational excitation of ClO is rationalized by a strong dependence of the excited upper PES on the Jacobi angle γ of the internuclear axis r of the ClO fragment with the separation coordinate R connecting the centers of mass of Cl and the ClO fragment. Time of flight measurements of selected rovibrational states yield the anisotropy of the fragmentation process, which is characterized by a positive β parameter of 0.35 ± 0.15. From this value the symmetry of the upper excited state was unequivocally determined to be B_2 in agreement with the theoretical work of Toniolo *et al.* Mixing of the initially excited $^1B_2$ surface with the nearby lying $^1A_2$ surface is likely due to the observation of ClO in the $^2\Pi_{1/2}$ manifold and is likely to explain the quantitative difference between calculated and measured anisotropy parameters. The decay is fast; calculated PES suggest a decay within 50 fs, and the experimental observation only allows to define an upper limit of 300 fs. Some discrepancies remain between theoretical work and experimental observations for shorter dissociation wavelengths.

ACKNOWLEDGMENTS

This work has been supported by the Deutsche Forschungsgemeinschaft and the Fonds der Chemischen Industrie. The stay of Y.N. in Germany was granted by the JSPS-Program (Japanese Society for the Promotion of Science).

[1] J. G. Anderson, D. W. Toohey, and W. H. Brune, Science **251**, 39 (1991).
[2] S. Solomon, Nature (London) **347**, 347 (1990).
[3] L. T. Molina and M. J. Molina, J. Phys. Chem. **91**, 433 (1987).
[4] M. J. Prather, M. B. McElroy, and S. C. Wolfsy, Nature (London) **312**, 227 (1984).
[5] S. L. Nickolaisen, C. E. Miller, S. P. Sander, M. R. Hand, I. H. Williams, and J. S. Francisco, J. Chem. Phys. **104**, 2857 (1996).
[6] J. B. Burkholder, J. Geophys. Res. **98**, 2963 (1993).
[7] M. P. Gane, N. A. Williams, and J. R. Sodeau, J. Chem. Soc., Faraday Trans. **93**, 2747 (1997).
[8] J. J. Renard and H. I. Bolker, Chem. Rev. **76**, 488 (1976) and references therein.
[9] Y. Xu, A. R. McKellar, J. B. Burkholder, and J. J. Orlando, J. Mol. Spectrosc. **175**, 68 (1996).
[10] T. Shimanouchi, in *NIST Chemistry WebBook*, NIST Standard Reference Database No. 69, edited by W. G. Mallard and P. J. Linstrom (National Institute of Standards and Technology, Gaithersburg MD, 2000) (http://webbook.nist.gov).
[11] M. Nakata, M. Sugie, H. Takeo, C. Matsumura, F. Fukuyama, and K. Kuchitsu, J. Mol. Spectrosc. **86**, 241 (1981).
[12] *NIST-JANAF. Thermochemical Tables*, edited by M. W. Chase Jr., J. Phys. Chem. Ref. Data Monogr. 9 (NIST, Washington, D.C., 1998).
[13] H. F. Davis and Y. T. Lee, J. Chem. Phys. **105**, 8142 (1996).
[14] C. M. Nelson, T. A. Moore, M. Okumura, and T. K. Minton, Chem. Phys. **100**, 8055 (1994).
[15] T. A. Moore, M. Okumura, and T. K. Minton, J. Chem. Phys. **107**, 3337 (1997).
[16] Y. Tanaka, M. Kawasaki, Y. Matsumi, H. Fujiwara, T. Ishiwata, L. J. Rogers, R. N. Dixon, and M. N. R. Ashfold, J. Chem. Phys. **109**, 1315 (1998).
[17] M. Roth, T. Einfeld, K.-H. Gericke, and C. Maul, Phys. Chem. Earth **C26**, 513 (2001).
[18] M. Roth, Dissertation.de, Berlin, 2001.
[19] R. N. Zare, Mol. Photochem. **4**, 1 (1972).
[20] J. E. Del Bene, J. D. Watts, and R. J. Bartlett, Chem. Phys. Lett. **246**, 541 (1995).
[21] A. Toniolo, M. Persico, and D. Pitea, J. Phys. Chem. A **104**, 7278 (2000).
[22] C. Collaveri, G. Granucci, M. Persico, and A. Toniolo, J. Chem. Phys. **115**, 1251 (2001).
[23] R. Aures, K.-H. Gericke, M. Kawasaki, C. Maul, Y. Nakano, G. Trott-Kriegeskorte, and Z. Wang, Phys. Chem. Commun. **22**, 1 (2001).
[24] M. J. Cooper, T. Diez-Rojo, L. J. Rogers, C. M. Western, M. N. R. Ashfold, and J. W. Hudgens, Chem. Phys. Lett. **272**, 232 (1997).
[25] D. H. A. ter Stegge, M. Smits, C. A. de Lange, N. P. C. Westwood, J. B. Peel, and L. Visscher, Faraday Discuss. **115**, 259 (2000).
[26] W. B. DeMore, S. P. Sander, D. M. Golden, R. F. Hampson, M. J. Kurylo, C. J. Howard, A. R. Ravishankara, C. E. Kolb, and M. J. Molina, *Chemical Kinetics and Photochemical Data for Use in Stratospheric Modelling Evaluation Number 11*, JPL Publication No. 94-26 (Jet Propulsion Laboratory, Pasadena, 1994).
[27] E. Rühl, A. Jefferson, and V. Vaida, J. Phys. Chem. **94**, 2990 (1990).
[28] M. Roth, C. Maul, and K.-H. Gericke, J. Chem. Phys. **107**, 10 582 (1997).
[29] T. Haas, K.-H. Gericke, C. Maul, and F. J. Comes, Chem. Phys. Lett. **108**, 202 (1993).
[30] G. H. Cady, Inorg. Synth. **5**, 156 (1957).
[31] R. F. Delmdahl, S. Baumgärtel, and K.-H. Gericke, J. Chem. Phys. **104**, 2883 (1996).
[32] J. A. Coxon, Can. J. Phys. **57**, 1538 (1979).
[33] G. Herzberg, *Molecular Spectra and Molecular Structure, Vol. I: Spectra of Diatomic Molecules* (Van Nostrand, New York, 1950).
[34] X. Chen, R. Marom, S. Rosenwaks, I. Bar, T. Einfeld, C. Maul, and K.-H. Gericke, J. Chem. Phys. **114**, 9033 (2001).
[35] A. B. Cornford, D. C. Frost, F. G. Herring, and C. A. McDowell, J. Chem. Phys. **55**, 2820 (1971).
[36] F. Motte-Tollet, J. Delwiche, J. Heinesch, M.-J. Hubin-Franskin, J. M. Gingell, N. C. Jones, N. J. Mason, and G. Marston, Chem. Phys. Lett. **284**, 452 (1998).
[37] R. Bersohn and S. H. Lin, Adv. Chem. Phys. **16**, 67 (1969).
[38] G. E. Busch and K. R. Wilson, J. Chem. Phys. **56**, 3638 (1972).
[39] R. Schinke, *Photodissociation Dynamics* (Cambridge University Press, Cambridge, 1993).